Sara Fernández-Lizarbe[a], Emilio Lecona[a,b], Angélica Santiago-Gómez[c], Nieves Olmo, María Antonia Lizarbe and Javier Turnay*

Structural and lipid-binding characterization of human annexin A13a reveals strong differences with its long A13b isoform

DOI 10.1515/hsz-2016-0242
Received June 30, 2016; accepted September 22, 2016; previously published online September 26, 2016

Abstract: Annexin A13 is the founder member of the vertebrate family of annexins, which are comprised of a tetrad of unique conserved domains responsible for calcium-dependent binding to membranes. Its expression is restricted to epithelial intestinal and kidney cells. Alternative splicing in the N-terminal region generates two isoforms, A13a and A13b, differing in a deletion of 41 residues in the former. We have confirmed the expression of both isoforms in human colon adenocarcinoma cells at the mRNA and protein levels. We have cloned, expressed, and purified human annexin A13a for the first time to analyze its structural characteristics. Its secondary structure and thermal stability differs greatly from the A13b isoform. The only tryptophan residue (Trp^{186}) is buried in the protein core in the absence of calcium but is exposed to the solvent after calcium binding even though circular dichroism spectra are quite similar. Non-myristoylated annexin A13a binds in a calcium-dependent manner to acidic phospholipids but not to neutral or raft-like liposomes. Calcium requirements for binding to phosphatidylserine are around 6-fold lower than those required by the A13b isoform. This fact could account for the different subcellular localization of both annexins as binding to basolateral membranes seems to be calcium-dependent and myristoylation-independent.

[a]**Sara Fernández-Lizarbe and Emilio Lecona:** These authors contributed equally to this work.
[b]Present address: Genomic Instability Group, Centro Nacional de Investigaciones Oncológicas, E-28029 Madrid, Spain.
[c]Present address: Breast Cancer Research Group, Institute of Cancer Sciences, University of Manchester, Manchester, M20 4QL, UK.
***Corresponding author: Javier Turnay,** Departamento de Bioquímica y Biología Molecular I, Facultad de Ciencias Químicas, Universidad Complutense, E-28040 Madrid, Spain, e-mail: turnay@ucm.es
Sara Fernández-Lizarbe, Emilio Lecona, Angélica Santiago-Gómez, Nieves Olmo and María Antonia Lizarbe: Departamento de Bioquímica y Biología Molecular I, Facultad de Ciencias Químicas, Universidad Complutense, E-28040 Madrid, Spain

Keywords: annexin; calcium binding; circular dichroism spectroscopy; fluorescence emission spectroscopy; phospholipid binding; thermal stability.

Introduction

Annexins are a widely distributed multigene superfamily characterized by their ability to interact with biological membranes in a calcium dependent manner (Raynal and Pollard, 1994; Swairjo and Seaton, 1994; Gerke and Moss, 2002; Lizarbe et al., 2013). These proteins present a marked preference for interaction with acid phospholipids, mainly phosphatidylserine (PS), but differences are found among them regarding lipid composition, structure preferences and calcium requirements for the interaction. They are expressed by all living organisms, from protists to higher eukaryotes and plants, but with the exception of bacteria. However, the group of Fernandez and Morgan first reported the presence of a gene coding for a single domain annexin in the bacteria *Cytophaga hutchinsonii*, although the protein is not expressed (Morgan et al., 2006) and a broader survey of bacterial genomes has identified around 30 annexin homologs, including single-domain and multi-domain annexins in 17 bacterial species (Kodavali et al., 2014).

The annexin core shows a characteristic tetrad structure of homologous internal repeats (eight in annexin A6), domains of around 70 amino acids, with the overall shape of a slightly bent ring surrounding a central hydrophilic pore (Liemann and Huber, 1997). Calcium- and phospholipid-binding sites are located on the convex side while the N-terminus links domains I and IV on the concave side (Lizarbe et al., 2013). The N-terminus region shows great variability in length and amino acid sequence and it greatly influences protein stability and specific functions of annexins (Turnay et al., 2003a,b). Despite their gross structural similarity, annexins have diverged significantly in terms of their gene regulation, tissue-specific expression patterns, subcellular localization of different isoforms, and features peculiar to

individual annexins. Members of this family are involved in a wide range of intra and extracellular biological processes, most of them directly related with the conserved ability to bind to phospholipid bilayers. These functions involve membrane trafficking, exocytosis, endocytosis, membrane-cytoskeleton anchorage, regulation of membrane protein activities, membrane repair, calcium channel activity and regulation, and signal transduction (Raynal and Pollard, 1994; Swairjo and Seaton, 1994; Gerke and Moss, 2002; Lizarbe et al., 2013; Bouter et al., 2015). Even though annexins are mainly intracellular proteins and lack signal sequences for secretion, some of them (i.e. A1, A2 or A5) have been detected extracellularly, either secreted or attached to the outer membrane, where they may also exert some activities such as inhibition of blood coagulation, inhibition of neutrophil migration, interaction with extracellular proteins such as collagen or serum proteases, or even act as docking point for certain viruses. Annexins are also involved in a wide variety of pathological conditions ranging from cancer (i.e. annexins A2, A4 and several others) (Mussunoor and Murray, 2008; Wang and Lin, 2014; Wei et al., 2015), resistance to chemotherapy [annexin A13 (AnxA13)] (Reiske et al., 2010) to inflammation and autoimmunity (i.e. annexin A1, A2 or A5) (D'Acquisto et al., 2013; Misasi et al., 2015).

AnxA13 is considered as the founder member of the vertebrate family of annexins and the prototype for conserved evolutionary properties of this superfamily of proteins (Morgan et al., 1998; Iglesias et al., 2002). Alternative splicing of exon 2 yields two different isoforms, a long one (AnxA13b) and a short one whose mRNA lacks exon 2 that codes for a 41 amino acid cassette in the N-terminus (AnxA13a), which confers differential properties to these proteins (Lecat et al., 2000). Most vertebrate annexins are widely spread in all tissues although a few of them may be preferentially expressed in specific ones, as annexin A4 in epithelial cell-rich tissues (Kaetzel et al., 1989; Fiedler et al., 1995). Both AnxA13 isoforms have a specific tissue expression and they are only detected in gut and kidney (Wice and Gordon, 1992; Fiedler et al., 1995). Moreover, a unique characteristic among vertebrate annexins is that they are myristoylated *in vivo* in their N-terminal glycine residue although the recognition sites for N-myristoyltransferase (NMT) differ due to the loss of 41-residue cassette in AnxA13a. The predicted 17-residue sequences (Maurer-Stroh et al., 2002) for both AnxA13 isoforms are shown in Supplementary Figure 1. Although AnxA13 is an interesting target protein regarding enterocyte differentiation, its structure and function has been scarcely studied. In fact, the only structural/functional characterization of the recombinant long isoform has been carried out by our group (Turnay et al., 2005).

AnxA13a isoform was the first one discovered in HT-29 human colorectal carcinoma cells growing in the absence of glucose and using inosine as carbon source (Wice and Gordon, 1992), suggesting that AnxA13a could be a gene product involved in the specific differentiation process of colonocytes. However, no further reports have dealt with this isoform in human cells or tissues. Subcellular localization and potential function of both isoforms have been reported in epithelial polarized Madin-Darby Canine Kidney (MDCK) type II cells transfected with recombinant adenoviruses expressing AnxA13a, AnxA13b and non-myristoylated mutants. One of the most interesting differences between both AnxA13 isoforms is their different distribution in polarized epithelial cells. It has been described that AnxA13b is only located in the apical membranes whereas AnxA13a is distributed between the two plasma membrane domains but preferentially in the basolateral one (Lecat et al., 2000). The potential role of AnxA13b in apical transport of raft-containing vesicles from the trans-Golgi network has been also suggested (Fiedler et al., 1995; Lafont et al., 1998) as well as its interaction with the C2-domain of Nedd4 (ubiquitin protein ligase) directing it to the apical membrane (Plant et al., 2000). The short isoform is also partially associated to rafts in the apical membranes and, like AnxA13b, stimulates apical transport of influenza virus hemagglutinin. However, only AnxA13a seems to be involved in basolateral vesicle delivery (Lecat et al., 2000).

Immunolabeling of thin frozen sections of intestinal tissue has allowed the subcellular localization of different types of annexins, including AnxA2 (basolateral plasma membranes and the terminal web), AnxA4 (basolateral membranes) and AnxA13 (apical and basolateral membranes). Antibodies used for the localization of AnxA13 recognized both isoforms. Moreover, Western blot of intestinal tissue revealed the expression of both AnxA13 isoforms (Massey-Harroche et al., 1998; Massey-Harroche, 2000). Why do these cells require the expression of both the long and short forms of this annexin? In order to clarify this topic, we first need to characterize the structure and *in vitro* characteristics of both proteins. We have previously analyzed recombinant AnxA13b, but there is no structural or functional information regarding AnxA13a. Thus, in view of this lack of information supporting the physiological role of this annexin, we have cloned, expressed and purified human AnxA13a to investigate its structural properties and phospholipid-binding ability that could yield information to begin understanding the requirement of both isoforms in epithelial gastrointestinal cells.

Results

Expression of AnxA13a in human colorectal carcinoma cells

There is only one report on the expression of AnxA13a in human cells. The original report from 1992 (Wice and Gordon, 1992) described the expression of AnxA13a mRNA in HT-29 cells. Thus we used these cells together with Caco-2 cells to confirm the expression not only of this isoform but also the larger one, AnxA13b. We used specific primers to distinguish between isoforms 'a' and 'b' as well as a primer pair able to amplify both (Supplementary Figure 1). RT-PCR confirmed the expression of mRNA from both annexin isoforms in HT-29 and Caco-2 cells without showing significant differences in the expression between cell lines (Figure 1A). The only significant difference was found in the mRNA relative expression of the isoforms in Caco-2 cells (but not in HT-29 cells), where the AnxA13b/AnxA13a ratio was 2.2 ± 0.4 ($p < 0.05$). The expression of the protein isoforms was also verified by Western blot (Figure 1B). Again, no significant differences in the isoform ratio were detected in exponentially growing HT-29 cells whereas AnxA13b protein levels were 2-fold higher ($p < 0.05$) than those from AnxA13a in Caco-2 cells.

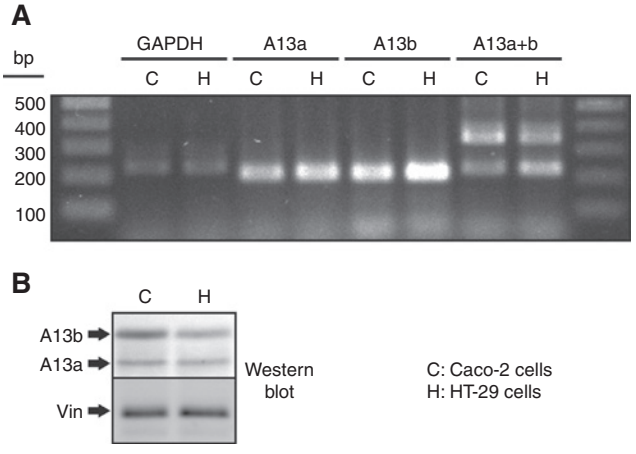

Figure 1: Expression of AnxA13 isoforms in human colorectal carcinoma cells.
(A) RT-PCR analysis of AnxA13 isoforms using specific (A13a and A13b) and generic (A13a+b) primer pairs. GAPDH mRNA expression was used as control. Expected band sizes are: GAPDH, 226 bp; A13a, 204 bp; A13b, 201 bp; A13a+b, 216 and 339 bp for isoform 'a' and 'b', respectively. (B) Western blot analysis of total cell homogenates from exponentially growing Caco-2 (C) and HT-29 (H) cells using a polyclonal antibody raised against AnxA13b. Vinculin expression is shown as control of even protein loading.

Circular dichroism analysis and thermal stability of purified recombinant AnxA13a

Due to the lack of information regarding the short annexin A13 isoform, and taking into account the reported different cellular behavior of both isoforms, we cloned, expressed in *E. coli*, and purified AnxA13a (Supplementary Figure 2). Circular dichroism (CD) spectrum of AnxA13a at 20°C in the far-UV region in the absence of calcium is shown in Figure 2A (A13a; solid line). The shape of the spectrum reflects a high α-helical percentage in the secondary structure of the protein, with two minima at 208 and 221 nm with molar ellipticities of –20.994 and –20.775 degrees·cm^2·dmol^{-1}, respectively. Accordingly, the CCA prediction indicates that the main contributions to the secondary structure are α-helix (80%), random coil (8%), and turns (12%) in good agreement with the secondary structure of the protein core of other annexins whose 3D structure is already known, and with the model that we proposed previously for the protein core of isoform AnxA13b (Turnay et al., 2005). The CD spectrum of AnxA13a significantly differs from that of the A13b isoform (Figure 2A) due to the random coil structure of the long N-terminal domain present in the A13b isoform which is absent in A13a. It also differs from the spectrum of AnxA5 (Figure 2A; A5) even though the percentages of secondary structure in the protein core are quite similar and both annexins present a very short N-terminus.

The addition of $CaCl_2$ up to 85 mM induced only a slight modification in the CD spectrum of AnxA13a (Figure 2A, dashed line). Secondary structure prediction did not reveal significant changes in the percentage of α-helix and the ratio $[\theta]^{221}/[\theta]^{208}$ was in both cases almost identical and close to 1, indicating that no variations in helix length were induced after saturation with calcium. The long AnxA13b isoform behaved in a similar way but showing a slight increase in α-helical content and helix length (Turnay et al., 2005) smaller than that detected in annexins A5 and A11 (Turnay et al., 2002; Lecona et al., 2003). Conversely, binding of calcium is accompanied by a hyperbolic increase in the melting temperature (T_m) from 50.0 ± 0.5°C in the absence of calcium (1 mM EGTA) up to 60.9 ± 0.4°C when saturated with this cation (85 mM $CaCl_2$), with a midpoint around 20 mM (Figure 2B, inset). This increase is specific for calcium, as it could not be reproduced by addition of $MgCl_2$ or NaCl at an equivalent ionic strength (Figure 2B, inset). The study of calcium binding in the absence of phospholipids requires the use of millimolar concentrations of $CaCl_2$, as it is well known that the affinity of annexins for this cation is around three

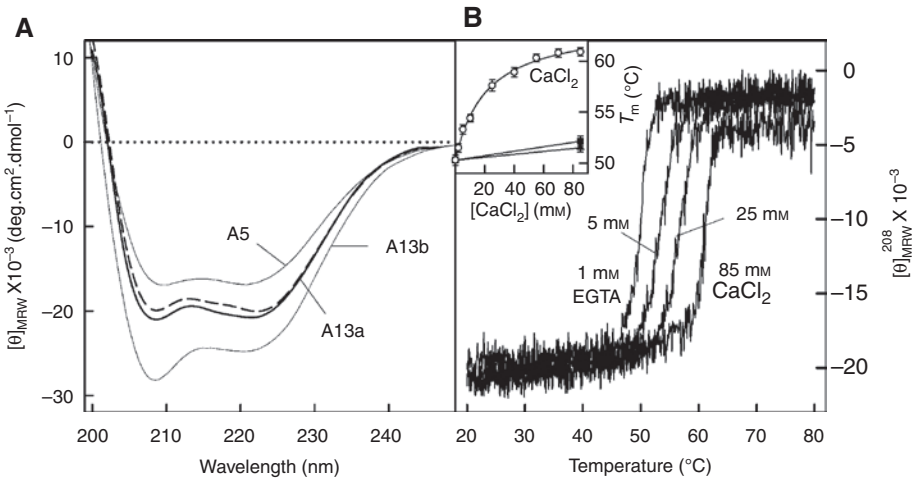

Figure 2: Far-UV circular dichroism spectra of AnxA13a.
(A) Far-UV CD spectra of AnxA13a (0.3 mg/ml) without calcium (solid line) and in the presence of 85 mM $CaCl_2$ (dashed line) at 20°C are shown in comparison with spectra from human annexin A5 and the A13b isoform. Spectra were registered in 20 mM Hepes, pH 7.4, containing 0.1 M NaCl. Each spectrum represents the average of six scans. (B) Influence of calcium binding on the thermal stability of annexin A13a. The figure shows only representative melting curves of AnxA13a in the absence (1 mM EGTA) and in the presence of increasing $CaCl_2$ concentrations (up to 85 mM) in 20 mM Hepes, pH 7.4, and 0.1 M NaCl. Melting points were determined from the inflection point of the first derivative of the smoothed melting curves using the Standard Analysis software from Jasco and data represent the means ± SD of at least two independent determinations at each $CaCl_2$ concentration. The inset shows the dependence of the T_m on $CaCl_2$ concentration (open circles). Black symbols show the effect of 85 mM $MgCl_2$ (square) or NaCl (triangle) at a concentration to obtain a protein solution with ionic strength equivalent to buffer containing 85 mM $CaCl_2$.

orders of magnitude lower under these conditions (Ayala-Sanmartin et al., 2000; Turnay et al., 2002). Thermal denaturation was followed by recording the molar ellipticity at 208 nm as a function of the temperature, as the main structural component of AnxA13a is α-helix. The melting curves showed a highly co-operative transition disregarding the calcium concentration used and the unfolding was always irreversible, as cooling of the denatured preparations did not recover the molar ellipticity values (not shown).

Fluorescence emission analysis

In order to analyze whether the tertiary structure surrounding the only Trp^{186} residue in AnxA13a is modified by calcium binding, we first registered fluorescence emission spectra with an excitation wavelength of 295 nm (Figure 3A) in the presence of different calcium concentrations, as the position of the emission maximum gives information regarding the exposition degree of the Trp residue. In the absence of calcium, the maximum is found at 320 nm but a significant red shift towards 344 nm is observed upon calcium binding that must arise from an increase in exposure to the polar solvent. Trp^{186} emission follows a hyperbolic dependence on calcium concentration in the ratio between intensities at 344 and 320 nm and in the position of the maximum (Figure 3B) with midpoint effects at 2.5 mM and 1.1 mM, respectively (which could be considered roughly as apparent dissociation constants), and are almost identical to those obtained for the long isoform (2.7 mM and 1.0 mM, respectively) (Turnay et al., 2005). Addition of 75 mM $MgCl_2$ only induced a slight change in the emission spectra with a 2 nm red-shift in the maximum and a minimal variation in the F^{344}/F^{320} intensity ratio, showing that the changes in the fluorescence emission spectra of Trp^{186} are calcium-specific. Moreover, we recorded Rayleigh scattering as a function of calcium or magnesium concentration and did not find significant variations indicating that these variations are not due to protein aggregation (Figure 3B, lower panel).

Acrylamide quenching of tryptophan emission

The exposure degree of Trp^{186} to the solvent can be quantified by means of dynamic fluorescence emission quenching experiments using acrylamide, which presents low accessibility to buried residues. The study was carried out in the absence (Figure 3C, continuous

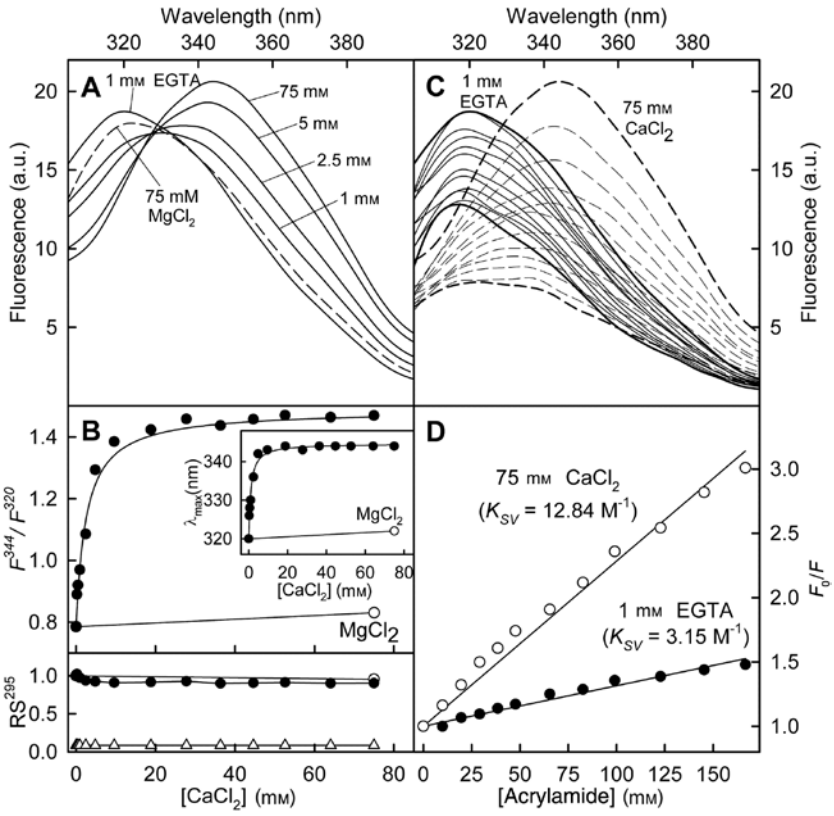

Figure 3: Fluorescence emission spectra of AnxA13a after calcium binding and acrylamide quenching of tryptophan emission. (A) Emission spectra at 295 nm excitation wavelength in the absence of calcium (1 mM EGTA) or at increasing $CaCl_2$ concentrations were registered at 20°C using a protein concentration of 0.2 mg/ml. Only spectra at representative calcium concentrations are shown. Fluorescence is expressed in arbitrary units (a.u.). (B) Variations in the F^{344}/F^{320} fluorescence intensity ratio of Trp^{186} and in the position of its emission maximum (inset) with calcium concentration (open circle, $MgCl_2$ instead of $CaCl_2$). The lower panel represents the Rayleigh scattering at 295 nm (RS^{295}) of buffer (up triangles) or AnxA13a at different calcium (black circles) or magnesium (open circle) concentrations. Data are normalized versus RS^{295} value from the AnxA13a preparation in the absence of calcium (EGTA 1 mM). (C) Fluorescence emission ($\lambda_{ex} = 295$ nm) at 20°C of Trp^{186} in AnxA13a (0.2 mg/ml) was quenched by sequential addition of a concentrated acrylamide stock solution up to 170 mM. Spectra in the absence of calcium (1 mM EGTA, continuous lines) and in the presence of 75 mM $CaCl_2$ (dashed lines) are shown. (D) Fluorescence intensity at 320 nm (absence of calcium; filled circles) or at 344 nm (75 mM $CaCl_2$; open circles) was determined and the data were plotted against acrylamide concentration according to the Stern-Volmer equation. Stern-Volmer constants (K_{SV}) are shown.

lines) and in the presence of 75 mM $CaCl_2$ (dashed lines) through analysis of the sensibility of fluorescence emission ($\lambda_{ex} = 295$ nm) to acrylamide quenching. Figure 3D shows the Stern-Volmer plots (F_0/F) using acrylamide concentrations that do not involve inner-filter effects (up to 170 mM). The decrease in intensity observed in the spectra in both cases, without altering the position of the maximum, confirmed the accessibility of acrylamide to the unique Trp residue of AnxA13a. The fluorescence emission data at the corresponding maximum (320 or 344 nm) were adjusted according to the Stern-Volmer equation as a function of acrylamide concentration, yielding quenching constants (K_{SV}) of 2.15 and 12.84 M^{-1} in the absence (1 mM EGTA) or presence of 75 mM $CaCl_2$, respectively.

Phospholipid binding

The interaction of AnxA13a with phospholipid vesicles was studied by ultracentrifugation after incubation of the protein with an excess of large unilamellar vesicles (400 nm in diameter) in the absence (1 mM EGTA) or presence of 150 μM $CaCl_2$ (Figure 4A). The vesicle pellets and supernatants were analyzed separately by SDS-PAGE. In the absence of phospholipid vesicles, protein sedimentation is minimal disregarding the absence of presence of calcium (Figure 4A, upper panel). The same effect is observed when liposomes with different composition are included in the absence of calcium; no interaction is detected between recombinant AnxA13a and vesicles. When calcium was added at 150 μM, recombinant

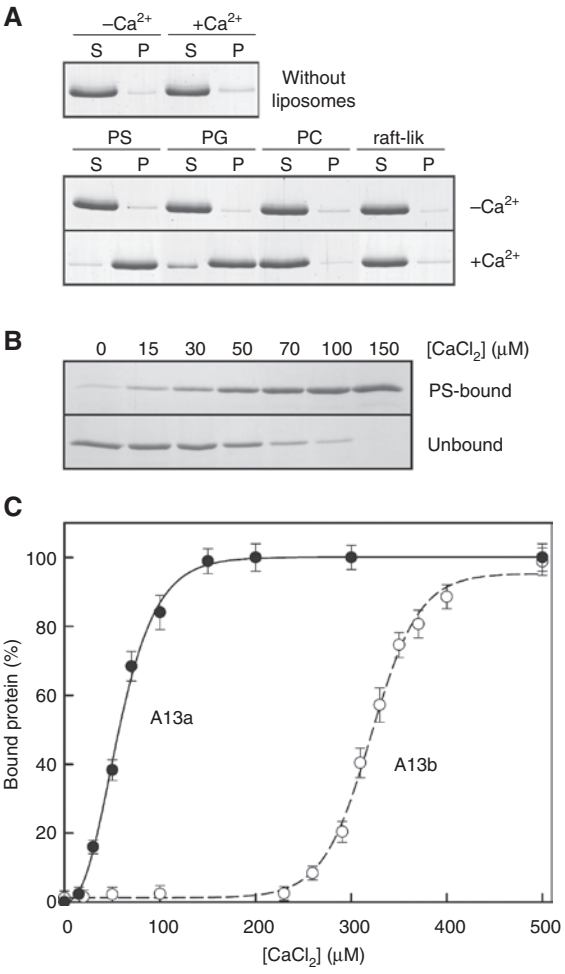

Figure 4: Binding of AnxA13a to liposomes with different lipid composition.
(A) The binding of recombinant AnxA13a to 400 nm unilamellar liposomes with different lipid composition [PS, PG, PC and PC:sphingomyelin:cholesterol in the ratio 1 : 1 : 1 (raft-like)] was performed by ultracentrifugation in the absence of calcium (1 mM EGTA; $-Ca^{2+}$) or in the presence of 150 μM $CaCl_2$ ($+Ca^{2+}$) with a lipid/protein molar ratio of 800 : 1. AnxA13a in the supernatants (S) and in the pellets (P) was analyzed by SDS-PAGE followed by Coomassie blue staining; representative gels are given. (B, C) The influence of calcium concentration on the binding of AnxA13a to 400 nm PS vesicles was analyzed as in (A) but using $CaCl_2$ concentrations ranging from 0 (1 mM EGTA) to 500 μM. A representative gel is shown in (B) and the densitometric analysis is shown in (C; black circles) compared to that of AnxA13b (open circles). Data represent mean values ± SD of three independent experiments.

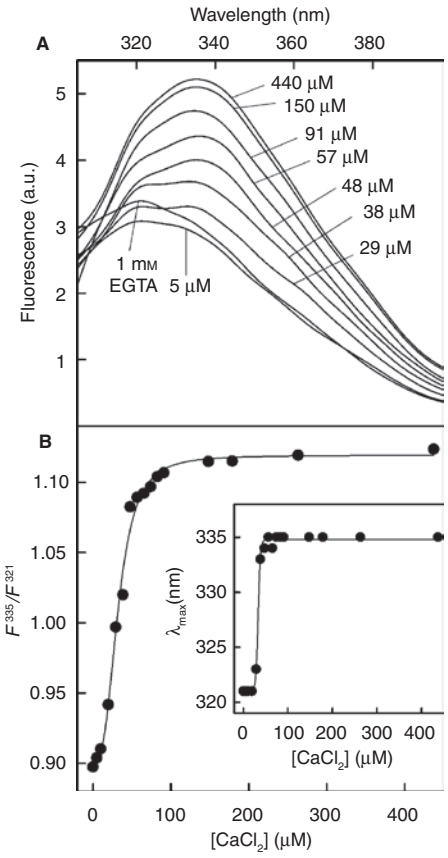

Figure 5: Calcium-dependent changes in the fluorescence emission spectra of AnxA13a in the presence of PS liposomes.
(A) Emission spectra at 295 nm excitation wavelength in the absence of calcium (1 mM EGTA) or at increasing $CaCl_2$ concentration were registered at 20°C in the presence of 50 nm unilamellar vesicles using a lipid/protein ratio of 800 : 1 (protein concentration: 0.05 mg/ml or 1.4 μM). Only spectra at representative calcium concentrations are shown. Fluorescence is expressed in arbitrary units (a.u.). (B) Variation in the $F^{335}/F2^{321}$ fluorescence intensity ratio of Trp^{186} and in the position of its emission maximum (inset) with calcium concentration.

AnxA13a was quantitatively bound to PS vesicles and >85% to phosphatidylglycerol (PG), but no binding was detected to phosphatidylcholine (PC) or raft-like vesicles (Figure 4A, lower panels).

A more detailed analysis of the calcium dependence of AnxA13a binding to PS vesicles is shown in Figure 4B and C. The binding of AnxA13a follows a sigmoidal pattern with a midpoint at 58 ± 4 μM $CaCl_2$, slightly higher than that described for other annexins as AnxA5 or A11 (around 20 μM) (Lecona et al., 2003; Turnay et al., 2009; Lizarbe et al., 2013), but much lower than that obtained for the long AnxA13b isoform (319 ± 7 μM $CaCl_2$) (Figure 4C).

Binding of AnxA13a to PS membranes was also studied by recoding Trp^{186} fluorescence emission spectra of the recombinant protein in the presence of unilamellar vesicles (50 nm in diameter) at a constant lipid to protein molar ratio (800 : 1) and increasing $CaCl_2$ concentrations (Figure 5). The addition of PS vesicles in the absence of calcium (1 mM EGTA) did not alter the overall shape of the spectrum, which showed a maximum at 321 nm (instead of 320 nm in the absence of phospholipids) (Figure 5A).

When calcium was sequentially added to the protein/PS mixture, a shift in Trp^{186} maximum position towards 335 nm was first observed with the apparent existence of two Trp populations (Figure 5A and B inset). An increase in the quantum yield was also observed that reached a maximum at $CaCl_2$ concentration above 150 μM. These changes also affected the F^{335}/F^{321} fluorescence ratio, which showed a sigmoidal increase with a midpoint at 29 ± 3 μM $CaCl_2$ quite similar to that observed for the shift in the position of the maximum (midpoint at 33 ± 4 μM) although the latter showed a sharper transition.

Induction of vesicle aggregation was analyzed using PS vesicles at different protein and calcium concentrations. However, no aggregation was induced by the recombinant protein even at high protein (2 μM) or calcium concentrations (1 mM $CaCl_2$).

Discussion

We have verified that the short AnxA13 isoform is indeed expressed in human colorectal adenocarcinoma cells. AnxA13a mRNA was detected by RT-PCR in exponentially growing HT-29 and Caco-2 cells even without the requirement of glucose deprivation as initially described in HT-29 cells. Both isoforms were detected and, although a quantitative analysis was not carried out, mRNA levels were quite similar in HT-29 cells and only a slight prevalence of AnxA13b mRNA was observed in Caco-2 cells (around 2-fold). Moreover, protein expression was also detected by Western blot and the relative expression levels qualitatively agreed with those observed in mRNA. When AnxA13a was first reported in HT-29 cells, the mRNA from this short isoform was detected as the primary transcription product. Our results differ from these original data as we detect equal amounts of mRNA from both AnxA13 isoforms in HT-29 cells in the absence of differentiation-inducing treatments. Wice and Gordon (1992) also reported on the lack of AnxA13 mRNA in Caco-2 cells, either proliferating or postconfluent. However, here we clearly demonstrate that these cells also express AnxA13a mRNA and protein, although in a slightly lower extent than that corresponding to the long isoform AnxA13b. In addition, expression levels are qualitatively similar to those expressed by proliferating HT-29 cells. In any case, these results do not contradict the potential role of AnxA13a in colonocyte differentiation as Caco-2 cells are also able to differentiate. On the contrary, they open a potential future line of research to analyze whether AnxA13a is involved or required for colonocyte differentiation, or if the ratio between both isotypes is somehow related or dependent on the proliferative or differentiation stage of the cells.

The structural characterization and analysis of the phospholipid binding ability of non-myristoylated AnxA13a was carried out with the recombinant protein, comparing it with the long isoform previously characterized by our group (Turnay et al., 2005), in order to determine the influence of the 41 amino acid cassette in the properties of annexin A13 as well as in calcium binding. Purification of recombinant AnxA13a followed a protocol quite similar to that described for other members of the annexin family due to its affinity for acidic phospholipids (Arboledas et al., 1997).

As for the purification of AnxA13b (Turnay et al., 2005), the short isoform also required a higher NaCl concentration to extract the protein from the vesicles, emphasizing the importance of ionic interactions in membrane binding (Campos et al., 1998; Montaville et al., 2002). Circular dichroism of AnxA13a reveals that the protein is correctly folded with an overall secondary structure quite similar to that reported for other annexins with a medium/short N-terminus, as AnxA5. CCA and other algorithms predict a secondary structure with a high α-helical content which has been described as a very stable arrangement. In fact, the T_m of AnxA13a in the absence of calcium is relatively high (around 50°C) and similar to other annexins with short N-terminus (Turnay et al., 2002). Interestingly, AnxA13b, whose protein core is identical to the short isoform, is much less stable with a T_m 6°C lower under equivalent experimental conditions (Turnay et al., 2005). This result clearly indicates that the longer N-terminal extension in AnxA13b, which is predicted as random coil (Turnay et al., 2005), can destabilize the protein core. This is not the case for other vertebrate annexins with an N-terminus with a similar length, as AnxA1 or AnxA2, whose thermal stability is even higher than that of short-tailed annexins probably due to the existence of α-helices in their N-terminus that strongly interact with the protein core in the absence of calcium as described for AnxA1 (around 60°C) (Rosengarth et al., 1999). The difference in thermal stability between both annexin A13 isoforms probably arises from slight modifications in the protein core structure and to the decrease in the overall α-helical content of the long isoform due to the destabilizing effect of the longer N-terminal extension in AnxA13b (Turnay et al., 2005). This fact could contribute to the functional differences between annexin A13 isoforms, for example, regarding the interaction with membranes via the convex core surface where the calcium and phospholipid binding domains are localized.

Saturation of AnxA13a with calcium did not significantly alter the CD spectrum of the protein, but it did strongly affect thermal stability in a concentration-dependent manner; the T_m of the protein increases 10°C. Thus, although the overall secondary structure of this annexin is mainly unaltered, changes in the loops connecting α-helices in the calcium binding regions of the convex surface must occur, as reported for other members of the annexin superfamily, that reinforce the stability of the protein core. These changes are clearly observed when the fluorescence emission spectra of the only Trp residue of the molecule is analyzed. Trp^{186} is in a position equivalent to Trp^{187} in annexin A5 according to sequence alignment and to the 3D-model that we previously reported for the AnxA13 protein core (Turnay et al., 2005) (Figure 6). In the absence of calcium, the position of the tryptophan emission maximum is 320 nm, which corresponds to a residue protected from the environment. This is in good agreement with the acrylamide quenching experiments in the absence of calcium that yield a low Stern-Volmer constant (3.15 M^{-1}), quite similar to that reported for the long isoform (2.99 M^{-1}) and only slightly higher

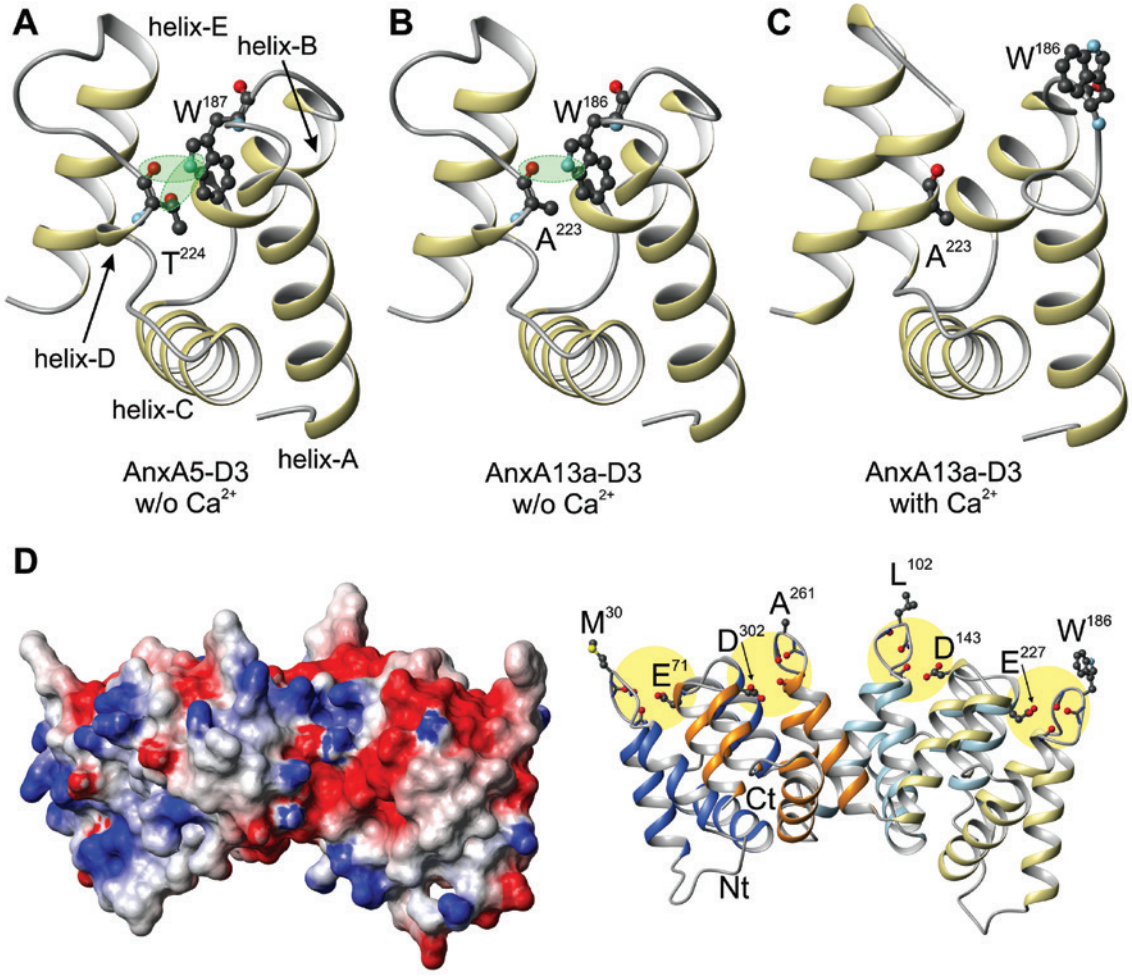

Figure 6: Three-dimensional model of annexin A13a.
Three-dimensional protein models of human AnxA13a in the absence (w/o Ca^{2+}) or in the presence (with Ca^{2+}) of calcium were obtained as described previously (Turnay et al., 2005) using the Swiss-Model Server. (A) Three-dimensional structure of domain III of human AnxA5 (residues 167–246) in the absence of calcium bound to this domain ('closed' conformation; PDB entry: 1AVH). Dotted lines and green shading mark hydrogen bonds responsible for static quenching of W^{187} fluorescence emission. Helices A to E are indicated. (B) Three-dimensional protein model of domain III of AnxA13a (residues 166–245) in the absence of calcium, and (C) in the 'high-calcium' form. (D) Full three-dimensional model predicted for AnxA13a in the presence of calcium. Left: van der Walls surface representation showing negatively charged (red), positively charged (blue) or hydrophobic surfaces. Right: ribbon representation showing the four protein domains in different colors as well as the main calcium binding regions (shadowed in yellow) with indication of the residues or carbonyl oxygen atoms potentially involved in calcium chelation. Hydrophobic residues protruding from the loops between helices A and B in the four domains are shown. The figure was prepared using the MOLMOL program (Koradi et al., 1996).

than that for human (0.39 M^{-1}) (Sopkova et al., 1998) and chicken (1.94 M^{-1}) (Arboledas et al., 1997) AnxA5. These data strongly support the notion that Trp^{186} in buried in a hydrophobic cleft when AnxA13a is in the calcium-free or 'closed' conformation as suggested by the 3D model (Figure 6B). Upon calcium binding, the environment of the Trp residue changes dramatically according to the modifications observed in the fluorescence emission spectra: a 24 nm red-shift and a significant increase in the quantum yield. The red-shift in the fluorescence emission maximum of Trp^{186} clearly indicates that it changes to an exposed environment; this fact is confirmed by the increased accessibility of acrylamide to this residue, with a high Stern-Volmer constant (12.84 M^{-1}) that corresponds to an almost completely exposed Trp residue (Lakowicz, 2006) and is again in agreement with the proposed structural model (Figure 6C). The quantum yield of a Trp residue exposed to the polar solvent should decrease due to dynamic quenching. However, AnxA13a behaves differently showing an increase in the quantum yield of Trp^{186} when it is exposed. A similar effect has been described for annexin A5 and has been attributed to the existence of static quenching of the Trp fluorescence due to the establishment of hydrogen bonds between the nitrogen atom of the indole ring and the hydroxyl and carbonyl oxygens of a threonine residue located in the loop between helices D and E in domain III of annexin A5 (Thr^{224}) (Sopkova-De Oliveira Santos et al., 2001) (Figure 6A). AnxA13a does not have a threonine residue in an equivalent position but, as observed in the 3D model structure of the protein core of AnxA13 (Turnay et al., 2005) (Figure 6B), this position is occupied by an alanine residue (Ala^{264} in AnxA13b and Ala^{223} in AnxA13a) whose carbonyl oxygen is at the right distance and orientation to establish a hydrogen bond with the indole ring of Trp^{186}.

Interestingly, changes in the environment of the Trp residue take place at lower calcium concentrations than those required for the overall structural/thermal stabilization. The midpoint concentration for the red-shift in the Trp emission maximum is 1.1 mM (2.5 mM for F^{344}/F^{320}) whereas the midpoint for the increase in the T_m is around 20 mM. This difference in calcium requirements strongly suggests that calcium may bind not only to the canonical type II calcium-binding domains located in the AB loops in each domain of AnxA13a (as suggested by the sequence alignment and the 3D-model; Figure 6D), but that additional calcium binding sites with lower affinity for this cation may also exist, as described in other vertebrate annexins, contributing not only to stabilize the annexin core but also increase the affinity for acidic phospholipids (Lizarbe et al., 2013).

As observed from the fluorescence emission spectra of AnxA13b in the presence of PS vesicles, the conformational change affecting the AB loop where Trp^{186} is located is required for the interaction. The spectra under these conditions also experiments a red-shift with an increase in the quantum yield in a calcium-dependent manner. But this changes take place at calcium concentrations two orders of magnitude lower than in the absence of PS vesicles (around 30 μM). The red-shift is 10 nm smaller than that observed in the absence of PS probably due to a partial protection of Trp^{186} from the polar solvent as this residue is partially inserted into the phospholipid bilayer; this could also explain the higher increase in the quantum yield upon interaction of AnxA13a with PS vesicles in the presence of calcium.

Experiments with MDCKII cells transfected with recombinant myristoylated and non-myristoylated AnxA13 isoforms clearly indicate that the myristoyl moiety is required for their association with lipid rafts which are mainly present in the apical membranes (Lecat et al., 2000). However, binding of AnxA13 to rafts requires not only myristoylation, but also calcium. In fact, Lafont and coworkers (Lafont et al., 1998) have reported that only half of the cellular pool of AnxA13b is bound to membranes when calcium is chelated. In agreement with this observation, we have described that, *in vitro,* myristoylated AnxA13b (but not the non-myristoylated form) partially binds to raft-like liposomes and to neutral or acidic phospholipids in the absence of calcium, but requires calcium for quantitative binding (Turnay et al., 2005). This is probably due to the weak interaction between myristoylated proteins and lipid bilayers, which show a Gibbs free binding energy of around 8 kcal/mol (Peitzsch and McLaughlin, 1993). Hence, binding of AnxA13 isoforms to rafts may require additional calcium-dependent interactions between the convex side of the protein core (where calcium-binding sites are located; Figure 6D) with the membranes either directly or through interactions with other membrane-bound proteins. In addition, as shown in Figure 6D, the convex surface of the calcium-bound conformation of both isoforms presents hydrophobic residues protruding from the loops between helices A and B in each domain (M^{30}, L^{102}, W^{186} and A^{261} in AnxA13a), which could contribute to strengthening binding to membranes.

In contrast to the subcellular localization of AnxA13b, which is only found associated to raft-like structures in the apical membrane of MDCKII cells, AnxA13a can be found not only in apical membrane domains, but also in the basolateral membranes of polarized epithelial cells. Myristoylation of AnxA13a is required for its apical delivery as transfection of MDCKII cells with non-myristoylated

AnxA13a showed that this mutant protein did not interact with lipid rafts, although it bound in a calcium-dependent manner to basolateral membranes (Lecat et al., 2000). Thus, binding to non-raft membranes *in vivo* (as the basolateral membranes of epithelial cells) probably does not take place via the N-myristoylated tail but only through the calcium and phospholipid binding sites located in the convex side of the protein core. Our data suggest that the different subcellular distribution of both AnxA13 isoforms is probably due to their significant differences regarding calcium requirements for binding to the acidic phospholipids present in the inner leaflet of basolateral membranes. Consequently, the high calcium concentrations required by AnxA13b would direct this isoform almost exclusively towards raft-containing vesicles that migrate apically.

The affinity of purified non-myristoylated AnxA13a for phospholipid vesicles reveals that this protein only interacts with acidic phospholipids (but not with PC or raft-like liposomes) in a calcium-dependent manner. As AnxA13a shows a relatively low calcium-requirement for binding to acidic membranes (similar to those of AnxA5), it may bind to non-raft containing vesicles directed towards the basolateral epithelial membrane, whereas this is not possible for the long isoform. *In vitro* binding requires calcium concentration in the low micromolar range, which would be higher than basal cytosolic free calcium (around 100 nM). However, one has to take into account that lipid composition in the secretory vesicles is more complex and also that protein-protein interactions may facilitate the process. In addition, as shown in Supplementary Figure 3, stimulation of epithelial cells produces localized calcium domains around the Golgi or the basolateral plasma membrane (Leipziger et al., 1996; Hofer, 2005; Dolman and Tepikin, 2006; Pizzo et al., 2011), which could facilitate the binding of AnxA13a to these membranes (although not being high enough for the binding of non-myristoylated AnxA13b).

In summary, the structural and phospholipid-binding characterization of AnxA13a has revealed that this AnxA13 short isoform is quite different both in structure and behavior compared to long AnxA13b. Interestingly, recombinant non-myristoylated AnxA13a is quite similar to annexin A5 regarding secondary structure, thermal stability, and calcium requirements for membrane binding. Surprisingly, even though the protein core of both isoforms of AnxA13 are identical in sequence, the extra 41 amino acids in the N-terminus of AnxA13b must be interfering with the phospholipid binding sites in the convex surface of the molecule. There is a huge difference in the calcium requirements for binding to PS vesicles between both isoforms which could account for their different subcellular localization.

Materials and methods

Protein expression and purification

The human AnxA13a expression construct pTrcA13Ha was a generous gift from Prof. M.P. Fernández and Dr. R.O. Morgan from the University of Oviedo (Spain). The encoding region of the cDNA (NM_004306) was inserted between NcoI and HindIII restriction sites of the expression vector pTrc99A (Amersham Biosciences, Barcelona, Spain) and the identity of the construct was verified by DNA restriction analysis and sequencing. JA221 *E. coli* cells were transformed with the expression construct pTrcA13Ha and grown in LB broth containing 100 μg/ml of ampicillin at 37°C until an OD_{600} of 0.5. Different induction times and temperatures after addition of 0.5 mM isopropyl β-D-thiogalactoside (IPTG) were studied. Protein production was high at short induction times at 37°C and recombinant AnxA13a was detectable by SDS-PAGE and Coomassie blue staining. Longer times did not increase the protein yield significatively; thus, 3 h induction at 37°C was chosen as the optimal conditions for protein expression. Purification of the recombinant protein was achieved taking advantage from the property of being able to reversibly interact with PS vesicles and following, with slight modifications, the method described for annexin A5 (Arboledas et al., 1997) and A13b (Turnay et al., 2005). The electrophoretic and Western blot analyses of the material from the main steps of the purification process are shown in Supplementary Figure 2A. Briefly, after centrifugation at 6000 *g* for 15 min, collected cells were resuspended in 50 mM Tris, pH 7.4, containing 0.1 M NaCl, 2.5 mM EGTA and 2 mM PMSF and ruptured by sonication cycles at 4°C (lane H). The homogenate was stirred at 4°C for 90 min and centrifuged at 27 000 *g* for 90 min at 4°C, allowing the solubilization of the recombinant protein with a high yield (lane S_0). The supernatant was mixed with PS-enriched vesicles (1 mg/ml final concentration; Sigma, Alcobendas, Spain) and 2 mM $CaCl_2$, and stirred for 30 min at 4°C. The mixture was centrifuged at 27 000 *g* for 45 min at 4°C; the main part of the bacterial proteins remained in the supernatant (lane S_1). The vesicle pellet was washed twice with 50 mM Tris, pH 7.4, containing 0.1 M NaCl and 2 mM $CaCl_2$. The recombinant protein was then extracted by resuspension of the vesicles in the presence of 50 mM Tris, pH 7.4, containing 5 mM EGTA and 0.25 M NaCl and further centrifugation (lane E). At this step, a major protein contaminant of around 45 kDa was still present together with unsedimented phospholipidic vesicles. Finally, the protein was purified first by DEAE-cellulose chromatography, after dialysis against 50 mM Tris, pH 7.4, 1 mM EGTA, and elution of AnxA13a using a linear NaCl gradient, and second by size-exclusion chromatography on a Sephadex G-75 column (Amersham Pharmacia Biotech, Buckhinghamshire, UK). Purified protein (lane A13a) was dialyzed versus 20 mM Hepes, pH 7.4, containing 0.1 M NaCl, and concentrated, when required, using Vivaspin centrifugal concentrators with a 10 000 Da molecular weight cut-out (Sartorius, Göttingen, Germany). Purification of AnxA5 and AnxA13b for comparative purposes was carried out in our laboratory according to the previously described protocols (Arboledas et al., 1997; Turnay et al., 2005).

The identity of the recombinant protein (AnxA13a) was confirmed by amino acid analysis (Beckman 6300 amino acid analyzer)

as well as N-terminal sequencing (12 residues) and MALDI-TOF MS (matrix-assisted laser-desorption ionization time-of-flight mass spectroscopy), as previously described (Turnay et al., 2005) (Supplementary Figure 2B). The molar absorption coefficient of AnxA13a at 280 nm was determined from the UV-visible spectra after subtraction of apparent absorption due to light scattering and determination of the protein concentration by amino acid analyses from aliquots directly taken from the cuvette ($E^{0.1\%} = 0.75$).

Circular dichroism spectroscopy

The far-UV CD spectra were monitored between 200 and 250 nm at 20°C in a Jasco J-715 spectropolarimeter equipped with a Neslab RTE-111 thermostat using 0.05 cm pathlength thermostatized cuvettes. Melting curves were obtained in 20 mM Hepes, pH 7.4, containing 0.1 M NaCl to avoid pH changes during heating. Changes in ellipticity at 208 nm were monitored between 20 and 80°C at 60°C/h. The effect of calcium on the far-UV CD spectrum and T_m was analyzed by employing protein samples with increasing $CaCl_2$ concentrations. Samples with equivalent maximal ionic strength, obtained by addition of NaCl or $MgCl_2$ instead of $CaCl_2$, were used as controls. Control samples without calcium always contained 1 mM EGTA. All spectra were averaged over six scans and were corrected by subtracting buffer contribution from parallel spectra in the absence of protein; units are expressed as mean residue weighed molar ellipticities ($[\theta]_{MRW}$). Prediction of the secondary structure from the far-UV CD spectra was performed using the convex constraint algorithm (CCA) as described by Perczel and coworkers (Perczel et al., 1992).

Fluorescence emission spectroscopy

Fluorescence emission spectra were recorded in an SLM Aminco 8000C spectrofluorimeter at 20°C. Trp emission was measured using an excitation wavelength of 295 nm in a 0.4 cm excitation pathlength and 1.0 cm emission pathlength cuvette. Spectra were monitored between 285 and 400 nm. Rayleigh scattering at 90° was obtained from the maximum at 295 nm of spectra recorded at this excitation wavelength. The effect of calcium was titrated by sequential addition of $CaCl_2$. Acrylamide quenching of Trp fluorescence was analyzed by recording emission spectra (295 nm excitation wavelength) at increasing acrylamide concentrations, and taking into account the effect of dilution as previously described (Lecona et al., 2003; Turnay et al., 2005). Care was taken to avoid the inner filter effect and that solutions presented always UV absorption below 0.04 at 295 nm. The quenching constant (K_{SV}) was calculated from the Stern-Volmer plot of F_0/F at the emission maximum against acrylamide concentration, according to the equation $F_0/F = 1 + K_{SV}[Q]$, where F_0 is the fluorescence intensity at zero quencher concentration and F the intensity at a given quencher concentration ([Q]).

Binding to phospholipids and vesicle aggregation assays

Unilamellar vesicles of PS (Avanti Polar Lipids, Alabaster, AL, USA), phosphatidylcholine (PC), phosphatidylglycerol (PG), and a raft-like mixture (PC : sphingomyelin : cholesterol 1 : 1 : 1) (all from Sigma except PS) were obtained by hydration of a thin dried-lipid film in 20 mM Hepes, pH 7.4, containing 0.1 M NaCl, followed by extrusion through polycarbonate filters of 100 or 400 nm pore diameter (Lipex Biomembranes, Vancouver, Canada). Small unilamellar vesicles (50 nm) were prepared from freshly obtained 400 nm vesicles by further extrusion through polycarbonate filters of the corresponding pore diameter.

The interaction of AnxA13a with 400 nm vesicles was carried out at a constant lipid/protein molar ratio of 800 : 1 with variable calcium concentrations in 20 mM Hepes, pH 7.4, containing 0.1 M NaCl at 20°C for 15 min. The final mixture (100 µl) was ultracentrifuged at 150 000 *g* and 4°C for 1 h (Optima Max-XP ultracentrifuge with a TLA 120.1 rotor; Beckman-Coulter, Brea, CA, USA). After separation of supernatant and pellet, protein was detected by Coomassie blue staining after SDS-PAGE. Phospholipid-free controls showed negligible sedimentation of annexin under these experimental conditions. Gels were scanned in a Gel Doc XR system from Bio-Rad (Alcobendas, Spain) and a densitometric analysis was performed, obtaining volumograms, using the QuantityOne v4.6.9 software.

Vesicle aggregation studies were carried out by recording absorption at 360 nm immediately after the addition of calcium to a mixture of unilamellar vesicles (100 nm; 0.1 mg/ml) and AnxA13a at 25°C. Calcium was added from a $CaCl_2$ stock solution, and absorption was registered in a thermostatically controlled cuvette for at least 10 min.

Cell culture, RT-PCR and Western blotting

Caco-2 (HTB-37) and HT-29 (HTB-38) human colorectal adenocarcinoma cells were obtained from the ATCC (American Type Culture Collection) and were cultured in DMEM (Dulbecco's modified Eagle's medium) containing 4.5 g/l glucose and supplemented with 10% heat-inactivated fetal calf serum, penicillin (100 IU/ml), streptomycin (100 µg/ml) and 2 mM glutamine. Cells were maintained in a humidified atmosphere of 5% CO_2 at 37°C and were routinely subcultured by trypsinization (0.05% trypsin, 0.02% EDTA).

RT (reverse transcriptase)-PCR analysis was carried out using total RNA isolated from exponentially growing cells using the ToTALLY RNA kit and the RETROscript RT-PCR kit, both from Ambion (Austin, TX, USA). The quality of the purified RNA was verified using a 2100 Bioanalyzer from Agilent (Santa Clara, CA, USA). PCR reactions were carried out in a GeneAmp PCR Sysytem (Applied Biosystems, Alcobendas, Spain) using the same amount of RT-template, AmpliTaq Gold PCR Master Mix (Invitrogen, Alcobendas, Spain) and primer pairs designed specifically for the amplification of AnxA13a, AnxA13b, both annexin isoforms simultaneously or GAPDH as control (Lecona et al., 2008) (Supplementary Figure 1).

Total cell protein extracts were obtained by solubilization of the monolayers in lysis buffer (10 mM Tris pH 8.0, 140 mM NaCl and 2% Triton X-100) containing protease inhibitors (Santiago-Gómez et al., 2013). Cell lysates were resolved by SDS-PAGE after heat denaturing in presence of 5% β-mercaptoethanol. Proteins were transferred to nitrocellulose membranes and analyzed by Western blot as described elsewhere (Lecona et al., 2003) using rabbit polyclonal anti-human AnxA13b or mouse monoclonal anti human vinculin (hVIN1, Sigma) antibodies followed by the corresponding secondary anti-rabbit IgG-HRP (Bio-Rad) or anti-mouse IgG-HRP (Pierce/Thermo Scientific, Rockford, IL, USA). Vinculin was used as protein loading control.

Polyclonal antibodies against recombinant human AnxA13b, that recognize both isoforms 'a' and 'b', were obtained as previously described (Turnay et al., 2005).

Other procedures

Protein concentration in pure preparations was determined from the UV-visible spectra, except for CD spectroscopy, where quantitative amino acid analysis was used. In cell extracts, protein concentration was determined using the DC Protein assay (Bio-Rad). The structural three-dimensional models of AnxA13a in the calcium-bound and unbound states were obtained using the Swiss-Model server as described previously (Turnay et al., 2005). Regression fitting of the experimental data to different equations and statistical analyses were performed using SigmaPlot software v.13 (Systat Software, San Jose, CA, USA).

Acknowledgments: We are thankful to the staff from the Genomics and Proteomics Center from the Complutense University of Madrid for their skillful assistance. This work was supported by the Ministerio de Ciencia e Innovación (MICINN), Spain (grant number BFU2008-04758).

References

Arboledas, D., Olmo, N., Lizarbe, M.A., and Turnay, J. (1997). Role of the N-terminus in the structure and stability of chicken annexin V. FEBS Lett. *416*, 217–220.

Ayala-Sanmartin, J., Vincent, M., Sopkova, J., and Gallay, J. (2000). Modulation by Ca^{2+} and by membrane binding of the dynamics of domain III of annexin 2 (p36) and the annexin 2-p11 complex (p90): implications for their biochemical properties. Biochemistry *39*, 15179–15189.

Bouter, A., Carmeille, R., Gounou, C., Bouvet, F., Degrelle, S.A., Evain-Brion, D., and Brisson, A.R. (2015). Review: annexin-A5 and cell membrane repair. Placenta *36* (Suppl. 1), S43–S49.

Campos, B., Mo, Y.D., Mealy, T.R., Li, C.W., Swairjo, M.A., Balch, C., Head, J.F., Retzinger, G., Dedman, J.R., and Seaton, B.A. (1998). Mutational and crystallographic analyses of interfacial residues in annexin V suggest direct interactions with phospholipid membrane components. Biochemistry *37*, 8004–8010.

D'Acquisto, F., Piras, G., and Rattazzi, L. (2013). Pro-inflammatory and pathogenic properties of Annexin-A1: the whole is greater than the sum of its parts. Biochem. Pharmacol. *85*, 1213–1218.

Dolman, N.J. and Tepikin, A.V. (2006). Calcium gradients and the Golgi. Cell Calcium *40*, 505–512.

Fiedler, K., Lafont, F., Parton, R.G., and Simons, K. (1995). Annexin XIIIb: a novel epithelial specific annexin is implicated in vesicular traffic to the apical plasma membrane. J. Cell Biol. *128*, 1043–1053.

Gerke, V. and Moss, S.E. (2002). Annexins: from structure to function. Physiol. Rev. *82*, 331–371.

Hofer, A.M. (2005). Another dimension to calcium signaling: a look at extracellular calcium. J. Cell Sci. *118*, 855–862.

Iglesias, J.M., Morgan, R.O., Jenkins, N.A., Copeland, N.G., Gilbert, D.J., and Fernández, M.P. (2002). Comparative genetics and evolution of annexin A13 as the founder gene of vertebrate annexins. Mol. Biol. Evol. *19*, 608–618.

Kaetzel, M.A., Hazarika, P., and Dedman, J.R. (1989). Differential tissue expression of three 35-kDa annexin calcium-dependent phospholipid-binding proteins. J. Biol. Chem. *264*, 14463–14770.

Kodavali, P.K., Dudkiewicz, M., Pikula, S., and Pawlowski, K. (2014). Bioinformatics analysis of bacterial annexins – putative ancestral relatives of eukaryotic annexins. PLoS One *9*, e85428.

Koradi, R., Billeter, M., and Wuthrich, K. (1996). MOLMOL: a program for display and analysis of macromolecular structures. J. Mol. Graph. *14*, 51-5, 29–32.

Lafont, F., Lecat, S., Verkade, P., and Simons, K. (1998). Annexin XIIIb associates with lipid microdomains to function in apical delivery. J. Cell Biol. *142*, 1413–1427.

Lakowicz, J.R. (2006) Quenching of fluorescence. In: Principles of Fluorescence Spectroscopy, J.R. Lakowicz, ed. (New York, USA: Springer), pp. 278–320.

Lecat, S., Verkade, P., Thiele, C., Fiedler, K., Simons, K., and Lafont, F. (2000). Different properties of two isoforms of annexin XIII in MDCK cells. J. Cell Sci. *113*, 2607–2618.

Lecona, E., Turnay, J., Olmo, N., Guzmán-Aránguez, A., Morgan, R.O., Fernández, M.P., and Lizarbe, M.A. (2003). Structural and functional characterization of recombinant mouse annexin A11: influence of calcium binding. Biochem. J. *373*, 437–449.

Lecona, E., Olmo, N., Turnay, J., Santiago-Gómez, A., López de Silanes, I., Gorospe, M., and Lizarbe, M.A. (2008). Kinetic analysis of butyrate transport in human colon adenocarcinoma cells reveals two different carrier-mediated mechanisms. Biochem. J. *409*, 311–320.

Leipziger, J., Nitschke, R., and Greger, R. (1996). Regulation of the intracellular calcium concentration in epithelial cells. Kidney Blood Press Res. *19*, 148–150.

Liemann, S. and Huber, R. (1997). Three-dimensional structure of annexins. Cell. Mol. Life Sci. *53*, 516–521.

Lizarbe, M.A., Barrasa, J.I., Olmo, N., Gavilanes, F., and Turnay, J. (2013). Annexin-phospholipid interactions. Functional implications. Int. J. Mol. Sci. *14*, 2652–2683.

Massey-Harroche, D. (2000). Epithelial cell polarity as reflected in enterocytes. Microsc. Res. Tech. *49*, 353–362.

Massey-Harroche, D., Mayran, N., and Maroux, S. (1998). Polarized localizations of annexins I, II, VI and XIII in epithelial cells of intestinal, hepatic and pancreatic tissues. J. Cell Sci. *111*, 3007–3015.

Maurer-Stroh, S., Eisenhaber, B., and Eisenhaber, F. (2002). N-terminal N-myristoylation of proteins: refinement of the sequence motif and its taxon-specific differences. J. Mol. Biol. *317*, 523–540.

Misasi, R., Capozzi, A., Longo, A., Recalchi, S., Lococo, E., Alessandri, C., Conti, F., Valesini, G., and Sorice, M. (2015). "New" antigenic targets and methodological approaches for refining laboratory diagnosis of antiphospholipid syndrome. J. Immunol. Res. *2015*, 858542.

Montaville, P., Neumann, J.M., Russo-Marie, F., Ochsenbein, F., and Sanson, A. (2002). A new consensus sequence for phosphatidylserine recognition by annexins. J. Biol. Chem. *277*, 24684–24693.

Morgan, R.O., Bell, D.W., Testa, J.R., and Fernández, M.P. (1998). Genomic locations of ANX11 and ANX13 and the evolutionary genetics of human annexins. Genomics *48*, 100–110.

Morgan, R.O., Martin-Almedina, S., Garcia, M., Jhoncon-Kooyip, J., and Fernandez, M.P. (2006). Deciphering function and mechanism of calcium-binding proteins from their evolutionary imprints. Biochim. Biophys. Acta *1763*, 1238–1249.

Mussunoor, S. and Murray, G.I. (2008). The role of annexins in tumour development and progression. J. Pathol. *216*, 131–140.

Peitzsch, R.M. and McLaughlin, S. (1993). Binding of acylated peptides and fatty acids to phospholipid vesicles: pertinence to myristoylated proteins. Biochemistry *32*, 10436–10443.

Perczel, A., Park, K., and Fasman, G.D. (1992). Analysis of the circular dichroism spectrum of proteins using the convex constraint algorithm: a practical guide. Anal. Biochem. *203*, 83–93.

Pizzo, P., Lissandron, V., Capitanio, P., and Pozzan, T. (2011). Ca^{2+} signalling in the Golgi apparatus. Cell Calcium *50*, 184–192.

Plant, P.J., Lafont, F., Lecat, S., Verkade, P., Simons, K., and Rotin, D. (2000). Apical membrane targeting of Nedd4 is mediated by an association of its C2 domain with annexin XIIIb. J. Cell Biol. *149*, 1473–1484.

Raynal, P. and Pollard, H.B. (1994). Annexins: the problem of assessing the biological role for a gene family of multifunctional calcium- and phospholipid-binding proteins. Biochim. Biophys. Acta *1197*, 63–93.

Reiske, H., Sui, B., Ung-Medoff, H., Donahue, R., Li, W.B., Goldblatt, M., Li, L., and Kinch, M.S. (2010). Identification of annexin A13 as a regulator of chemotherapy resistance using random homozygous gene perturbation. Anal. Quant. Cytol. Histol. *32*, 61–69.

Rosengarth, A., Rosgen, J., Hinz, H.J., and Gerke, V. (1999). A comparison of the energetics of annexin I and annexin V. J. Mol. Biol. *288*, 1013–1025.

Santiago-Gómez, A., Barrasa, J.I., Olmo, N., Lecona, E., Burghardt, H., Palacín, M., Lizarbe, M.A., and Turnay, J. (2013). 4F2hc-silencing impairs tumorigenicity of HeLa cells via modulation of galectin-3 and β-catenin signaling, and MMP-2 expression. Biochim. Biophys. Acta *1833*, 2045–2056.

Sopkova-De Oliveira Santos, J., Vincent, M., Tabaries, S., Chevalier, A., Kerboeuf, D., Russo-Marie, F., Lewit-Bentley, A., and Gallay, J. (2001). Annexin A5 D226K structure and dynamics: identification of a molecular switch for the large-scale conformational change of domain III. FEBS Lett. *493*, 122–128.

Sopkova, J., Vincent, M., Takahashi, M., Lewit-Bentley, A., and Gallay, J. (1998). Conformational flexibility of domain III of annexin V studied by fluorescence of tryptophan 187 and circular dichroism: the effect of pH. Biochemistry *37*, 11962–11970.

Swairjo, M.A. and Seaton, B.A. (1994). Annexin structure and membrane interactions: a molecular perspective. Annu. Rev. Biophys. Biomol. Struct. *23*, 193–213.

Turnay, J., Olmo, N., Gasset, M., Iloro, I., Arrondo, J.L., and Lizarbe, M.A. (2002). Calcium-dependent conformational rearrangements and protein stability in chicken annexin A5. Biophys. J. *83*, 2280–2291.

Turnay, J., Guzmán-Aránguez, A., Lecona, E., Pérez-Ramos, P., Fernández-Lizarbe, S., Olmo, N., and Lizarbe, M.A. (2003a). Influence of the N-terminal domain of annexins in their functional properties. Recent Res. Dev. Biochem. *4*, 53–78.

Turnay, J., Lecona, E., Guzmán-Aránguez, A., Pérez-Ramos, P., Fernández-Lizarbe, S., Olmo, N., and Lizarbe, M.A. (2003b). Annexins: structural characteristics of the N-terminus and influence on the overall structure of the protein. Recent Res. Dev. Biochem. *4*, 79–95.

Turnay, J., Lecona, E., Fernández-Lizarbe, S., Guzmán-Aránguez, A., Fernández, M.P., Olmo, N., and Lizarbe, M.A. (2005). Structure-function relationship in annexin A13, the founder member of the vertebrate family of annexins. Biochem J. *389*, 899–911.

Turnay, J., Guzmán-Aránguez, A., Lecona, E., Barrasa, J.I., Olmo, N., and Lizarbe, M.A. (2009). Key role of the N-terminus of chicken annexin A5 in vesicle aggregation. Protein Sci. *18*, 1095–1106.

Wang, C.Y. and Lin, C.F. (2014). Annexin A2: its molecular regulation and cellular expression in cancer development. Dis. Markers *2014*, 308976.

Wei, B., Guo, C., Liu, S., and Sun, M.Z. (2015). Annexin A4 and cancer. Clin. Chim. Acta *447*, 72–78.

Wice, B.M. and Gordon, J.I. (1992). A strategy for isolation of cDNAs encoding proteins affecting human intestinal epithelial cell growth and differentiation: characterization of a novel gut-specific N-myristoylated annexin. J. Cell Biol. *116*, 405–422.

Supplemental Material: The online version of this article (DOI: 10.1515/hsz-2016-0242) offers supplementary material, available to authorized users.